CoPt alloy grown on the WSe2(0001) van der Waals surface

Denys Makarov, Fabiola Liscio, Christoph Brombacher, Jean Paul Simon, Günter Schatz, Mireille Maret, Manfred Albrecht

CoPt alloy grown on the WSe_2(0 0 0 1) van der Waals surface

D. Makarov[a,*], F. Liscio[b], C. Brombacher[a,c], J.P. Simon[b], G. Schatz[a], M. Maret[b], M. Albrecht[a,c]

[a]*Department of Physics, University of Konstanz, D-78457 Konstanz, Germany*
[b]*SIMAP, INP Grenoble-CNRS-UJF, 1130 rue de la Piscine, BP 75, 38402 Saint Martin d'Heres, France*
[c]*Institute of Physics, Chemnitz University of Technology, D-09107 Chemnitz, Germany*

The structural and magnetic properties of 3-nm-thick CoPt alloys grown on WSe_2(0 0 0 1) at various temperature are investigated. Deposition at room temperature leads to the formation of a chemically disordered fcc CoPt alloy with [1 1 1] orientation. Growth at elevated temperatures induces $L1_0$ chemical order starting at 470 K accompanied with an increase in grain size and a change in grain morphology. As a consequence of the [1 1 1] growth direction, the CoPt grains can adopt one of the three possible variants of the $L1_0$ phase with tetragonal *c*-axis tilted from the normal to the film plane direction at 54°. The average long-range order parameter is found to be 0.35($\pm$0.05) and does not change with the increase in the deposition temperature from 570 to 730 K. This behavior might be related to Se segregation towards the growing facets and surface disorder effects promoted by a high surface-to-volume ratio. Magnetic studies reveal a superparamagnetic behavior for the films grown at 570 and 730 K in agreement with the film morphology and degree of chemical order. The measurements at 10 K reveal the orientation of the easy axis of the magnetization lying basically in the film plane.

Keywords: CoPt alloy; Magnetic anisotropy; $L1_0$ chemical ordering; Short-range ordering

1. Introduction

$L1_0$-ordered magnetic alloys such as CoPt and FePt have attracted much attention due to their high magneto-crystalline anisotropy and thus possible application as high-density magnetic recording media [1]. However, high annealing temperatures above 800 K for CoPt (FePt) alloys are required to induce the $L1_0$ chemical order [2]. Therefore, many studies are directed to lower the ordering temperature by growing alloys on appropriate buffer layers [3,4], utilizing surfactants to guide the formation of the anisotropic local order [5] or by deposition of multilayer nanocomposites [6–8]. Another approach employs He-ion beam irradiation, where a directional short-range chemical order present in pre-heated films is transformed into almost perfect chemical order after ion irradiation [9].

Recently, a reduction in ordering temperature was reported for $CoPt_3$(1 1 1) thin films grown on a low energy surface of WSe_2(0 0 0 1) [10,11]. A strong out-of-plane magnetic anisotropy was observed even in films grown at room temperature induced by the appearance of a short-range anisotropic chemical order driven by Se segregation. Note that this out-of-plane anisotropy direction is not expected neither in the disordered fcc structure nor in the $L1_2$-ordered $CoPt_3$(1 1 1) phase. This effect was also observed in thin $CoPt_3$(1 1 1) films grown on Pt(1 1 1) and Ru(0 0 0 1) at elevated deposition temperatures of about 690 K just before long-range $L1_2$-type chemical ordering sets in Refs. [12,13]. The presence of the out-of-plane anisotropy was also found in CoPt(1 1 1) films grown on Ru(0 0 0 1) [14].

*Corresponding author. Tel.: +49 7531 88 3861; fax: +49 7531 88 3090.
E-mail address: denys.makarov@uni-konstanz.de (D. Makarov).

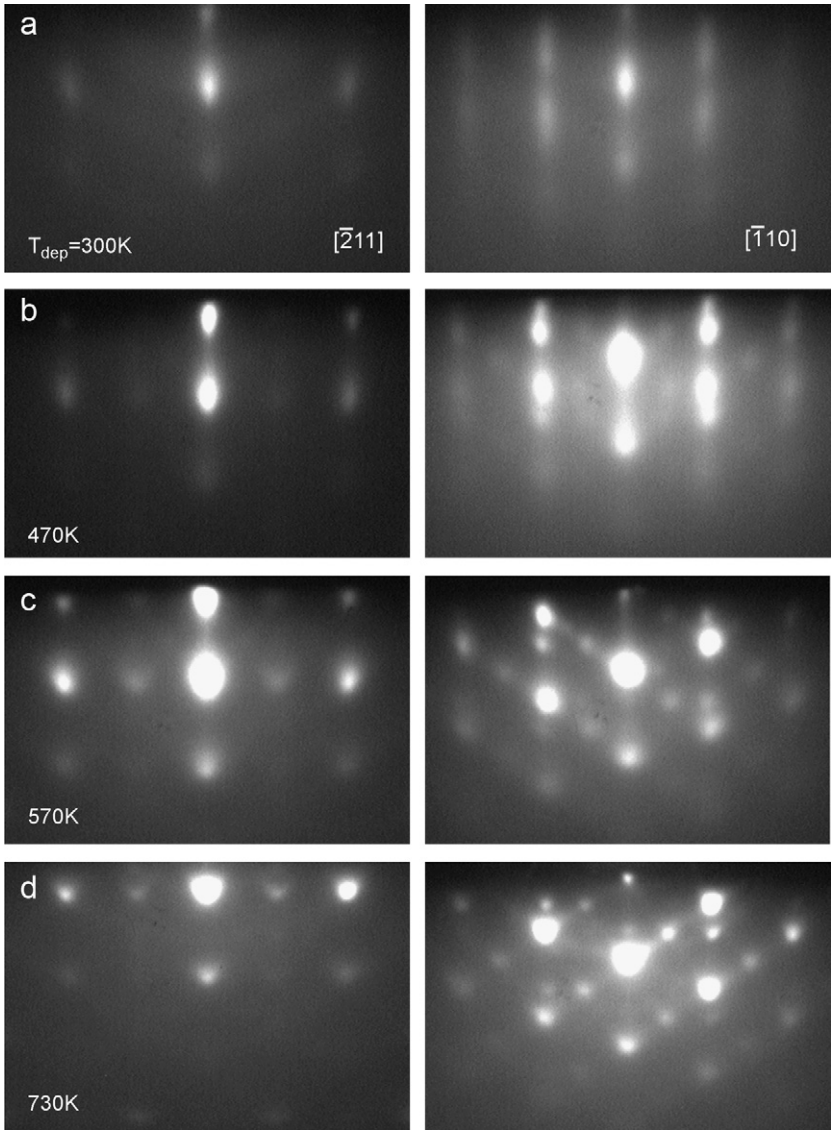

Fig. 1. RHEED patterns taken after the deposition of 3-nm-thick CoPt alloy on WSe_2(0 0 0 1) at various temperatures: (a) 300 K, (b) 470 K, (c) 570 K, and (d) 730 K.

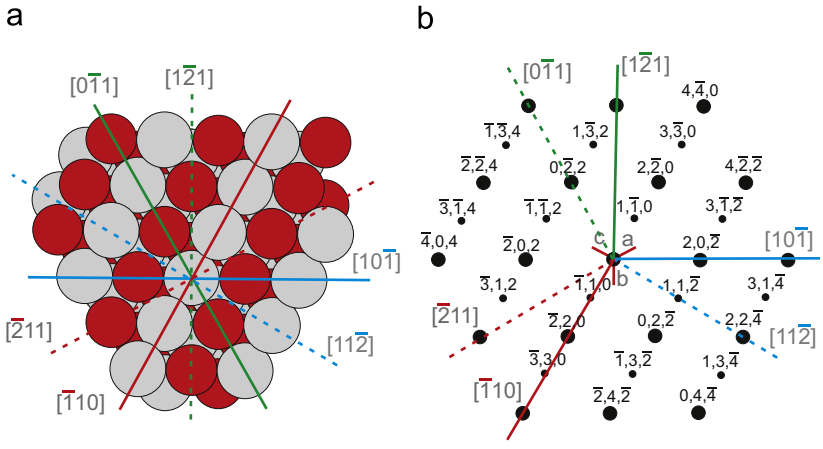

Fig. 2. (a) Schematic view of the (1 1 1) plane of the one variant of the $L1_0$ phase formed with the tetragonal axis along [0 0 1]; and (b) the reciprocal plane corresponding to the [1 1 1] zone axis.

In this work, we have investigated the growth, structure, and magnetic properties of CoPt deposits on $WSe_2(0\,0\,0\,1)$ grown at various temperatures. As the enthalpy change of the $L1_0$ CoPt phase formation ($\Delta H = -14\,kJ/mol$) is larger than that of $L1_0$ FePt ($\Delta H = -20\,kJ/mol$) [15], fully ordered CoPt films are more difficult to prepare than FePt [7,16,17]. As observed in Pt films deposited on $WSe_2(0\,0\,0\,1)$ [18], the high surfactant effect of Se atoms combined with strong Se interactions with Pt should have an influence on the growth kinetics of the CoPt alloys grown on $WSe_2(0\,0\,0\,1)$. In this case the local anisotropic order driven by Se segregation, could overcome the long-range L10 order and thus induce a perpendicular magnetic anisotropy. This approach was also studied for FePt films grown on $WSe_2(0\,0\,0\,1)$. However, independent on the deposition temperature an easy axis of magnetization lying in the film plane of the FePt(1 1 1) alloy was observed [19].

2. Experimental details

$WSe_2(0\,0\,0\,1)$ single crystals with a surface area in the size range of $1\,cm^2$ were grown in closed ampoules using the

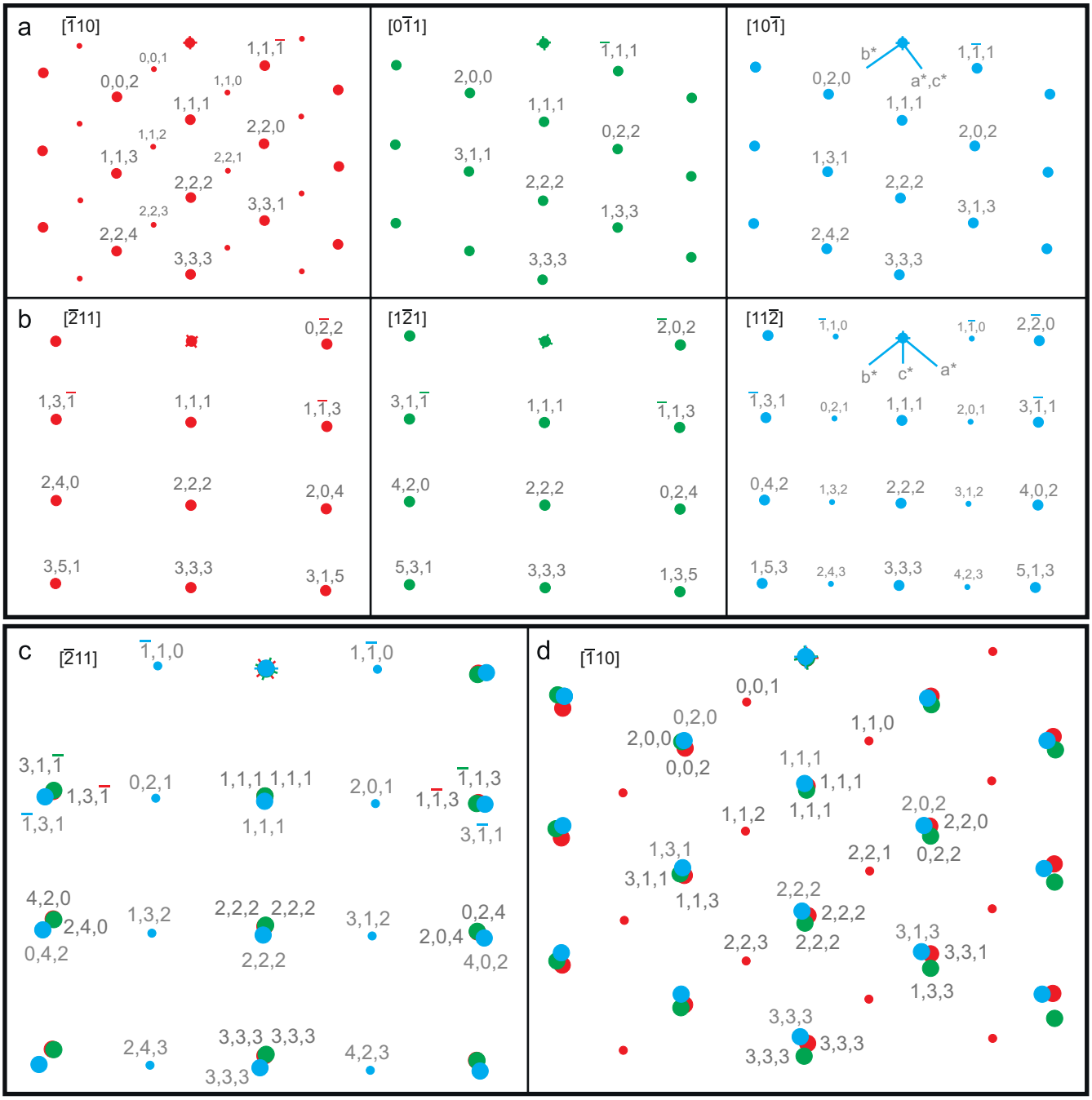

Fig. 3. The intensity contribution of the diffraction pattern of each of the three variants along the chosen azimuths (a) [$\bar{1}$ 1 0] and (b) [$\bar{2}$ 1 1] directions. The definition of the directions is given with respect to the variant presented in Fig. 2a. (c, d) The superimposition of the reflections coming from the three variants. The segments a^*, b^*, c^* correspond to the projections of the primitive vectors of the reciprocal lattice.

iodine vapor phase transport method [20]. WSe_2 is a metal chalcogenide semiconductor with a 2H-polytype layered structure, consisting of two-dimensional Se–W–Se sandwiches along the *c*-axis with an in-plane lattice constant of 3.28 Å and separated by a distance of 3.35 Å (van der Waals gap) [21,22]. As a result of this layered structure, the (0 0 0 1) surface of WSe_2 is chemically saturated and consists of close-packed hexagonally arranged Se atoms at the uppermost layer.

All substrates were cleaved prior being introduced into a molecular beam epitaxy (MBE) system equipped with two electron beam evaporators loaded with Co and Pt of purity greater than 99.99%. The pressure during deposition did not exceed 1×10^{-8} mbar. The composition of the deposited alloy was controlled during the growth with a mass spectrometer by adjusting the ratio between Co and Pt fluxes. The typical growth rates for Co and Pt were 0.02 and 0.029 Å/s, respectively.

The growth and structural properties of CoPt alloys were followed in-situ by reflection high-energy electron diffraction (RHEED). The surface morphology was characterized by UHV scanning tunneling microscopy (STM) using W tips electrochemically etched in NaOH diluted solution. All STM images were obtained in constant current mode at room temperature. Large angle X-ray diffraction measurements using a wavelength of 1.55 Å were carried out at the European Synchrotron Radiation Facilities (ESRF) in Grenoble on the seven-circle diffractometer of the BM02 beam line. Magnetic measurements were performed using a superconducting quantum interference device (SQUID) magnetometer with a maximal magnetic field of ± 5 T.

3. Structural characterization

During the co-deposition of Co and Pt at room temperature, RHEED imaging initially reveals the appearance of spots at specific positions which indicate epitaxial growth of fcc CoPt islands along the [1 1 1] direction. These spots become more pronounced with further film deposition. Fig. 1a shows the RHEED patterns after deposition of 3-nm-thick CoPt films taken along the two main azimuths $[\bar{2}\,1\,1]$ and $[\bar{1}\,1\,0]$ referring to CoPt(1 1 1). The spots are located on each side of the substrate streaks at distances consistent with the lattice mismatch of 17%. The epitaxial relationship between the substrate and CoPt film is as follows: $[1\,1\,\bar{2}\,0]WSe_2(0\,0\,0\,1)\|[\bar{1}\,1\,0]$CoPt(1 1 1) and $[1\,0\,\bar{1}\,0]WSe_2(0\,0\,0\,1)\|[\bar{2}\,1\,1]$CoPt(1 1 1). Based on a precise analysis of the RHEED patterns, the in-plane nearest neighbor distance for the CoPt film was found to be equal to 2.75 Å, which is slightly larger than the value found in the disordered bulk CoPt alloy (2.67 Å) indicating the presence of a residual epitaxial strain.

With increasing deposition temperature, intermediate RHEED spots start to appear for the CoPt film prepared at 470 K (Fig. 1b) and become more pronounced with further increase of the deposition temperature (Fig. 1c, d). These additional spots indicate the onset of $L1_0$-type chemical order in the CoPt(1 1 1) alloy. Since CoPt grains grow along the [1 1 1] direction, the three $\langle 0\,0\,1 \rangle$ directions, 54°-tilted with respect to the normal direction, are the potential growth directions for the tetragonal *c*-axis of the $L1_0$ phase. The arrangement of atoms in the (1 1 1) plane of one variant is schematized in Fig. 2a and the reciprocal plane corresponding to the [1 1 1] zone axis is presented in Fig. 2b. Using the software package CaRIne [23], the reflection pattern in Fig. 1d was simulated taking into account the presence of three variants (Fig. 3). Fig. 3a, b shows the diffraction patterns of these three variants along the $[\bar{1}\,1\,0]$ and $[\bar{2}\,1\,1]$ directions, which are defined with respect to the variant presented in Fig. 2a. It is important to point out that in both directions the superstructure spots can be produced by only one variant. The superimposition

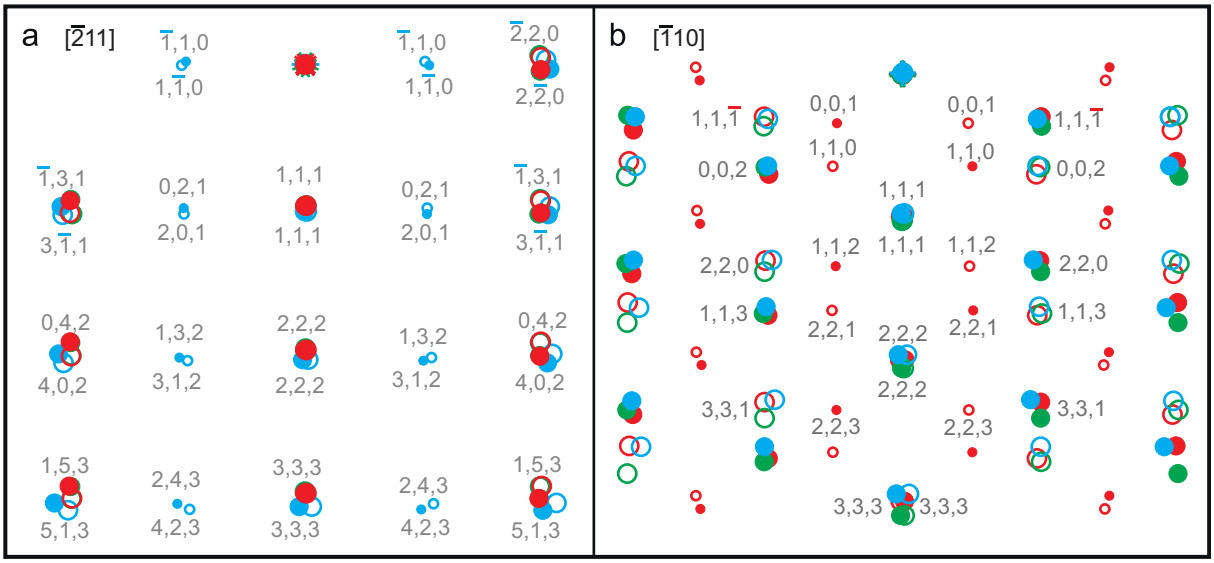

Fig. 4. The calculated diffraction pattern obtained from the superimposition of the reflections coming from the three variants and their twins of the $L1_0$ phase grown along the [1 1 1] direction.

of the two series of reciprocal planes is presented in Fig. 3c, d. The comparison with Fig. 1d shows that the twinning effect also has to be considered, as depicted in Fig. 4. However, superstructure spots of the associated twin phase are not observed in the RHEED images (Fig. 1c, d). This can be explained either by the weak intensities of the fundamental spots related to the twin, or by the weak twinning of the variant, which gives rise to the superstructure spots, as shown in Fig. 3. The latter is a peculiar feature of the $L1_0$ phase. The nearest neighbor distance in the (1 1 1) plane extracted from the RHEED patterns is equal to 2.68 Å, a value which is very close to the homoatomic and heteroatomic nearest pair distances of 2.69 and 2.65 Å, respectively, found in the bulk $L1_0$-CoPt(1 1 1) phase.

Scanning tunneling microscopy was used to follow the morphology of CoPt deposits. Consistent with the RHEED patterns, STM images confirm the three-dimensional island growth mode at all deposition temperatures. The lateral size, height, and shape of the individual grains strongly depend on the deposition temperature as shown in Fig. 5a–c. The increase in the lateral size and height of the individual CoPt islands with deposition temperature is summarized in Fig. 5d. The increase in island size is accompanied with a change in the grain shape due to the modification of the surface energies of the side-wall facets with chemical ordering. At room temperature a more rounded and even hexagonal shape of the grain is obtained, while at 730 K a tendency towards a more triangular shape is found. The triangular islands in Fig. 5c contain grain

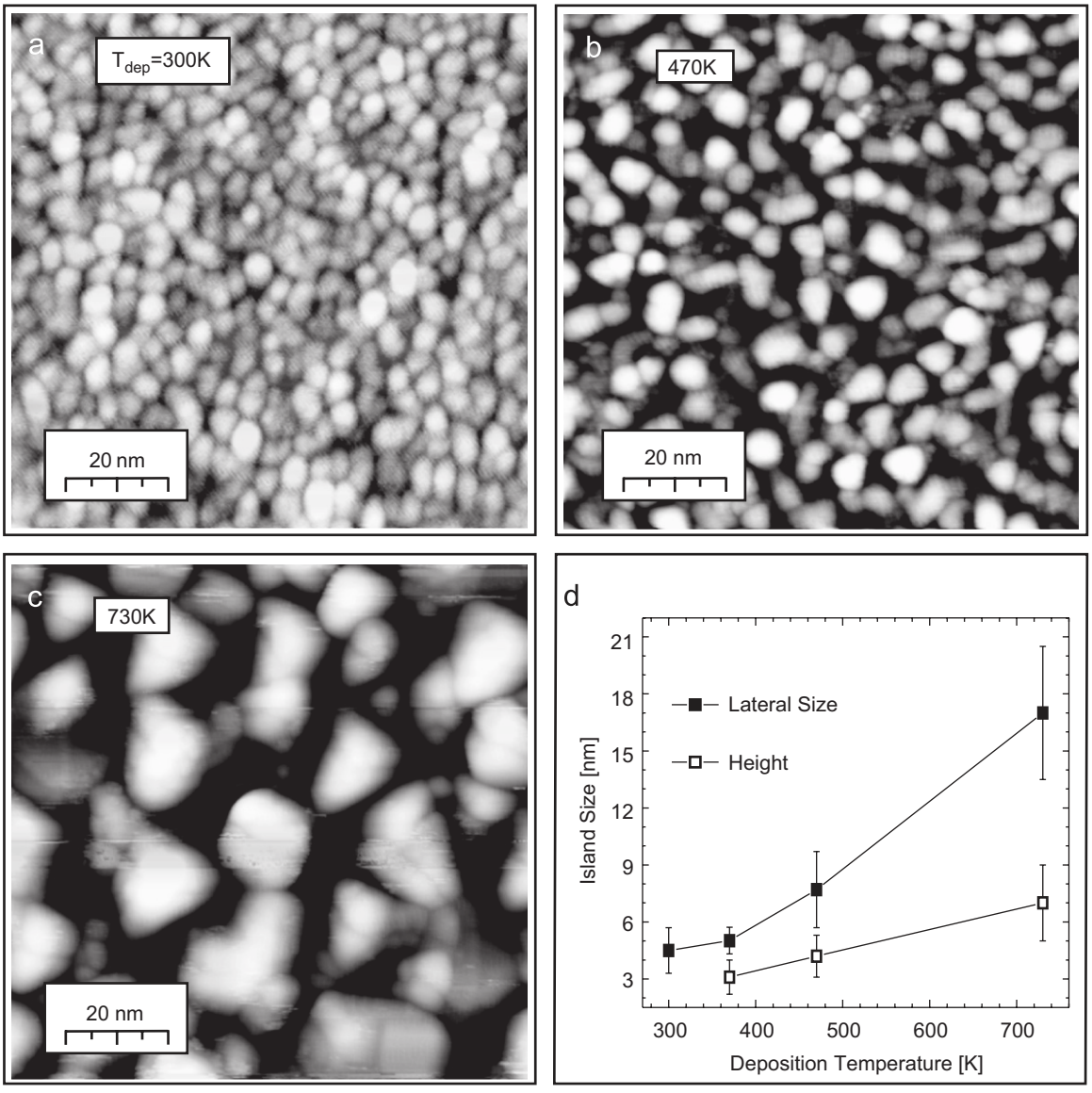

Fig. 5. Series of STM topographic images taken after the deposition of 3 nm-thick CoPt films on WSe_2(0 0 0 1) at various growth temperatures: (a) 300 K, (b) 470 K, and (c) 730 K. STM images are taken at room temperature with $U = 1.0$ V and $I = 0.1$ nA. (d) Grain's mean lateral size as a function of deposition temperature.

boundaries, that are attributed either to the existence of the three variants in the same island or more likely to the coalescence of several islands of different variants, since the equivalent side-wall facets {1 1 1} or {0 0 1} are differently decorated for $L1_0$ nanostructures. Note, that for $CrPt_3$(1 1 1) islands, adopting the $L1_2$ structure [24] such grain boundaries were not observed.

To determine the lattice parameters, chemical composition and the degree of $L1_0$-type chemical ordering, X-ray diffraction measurements in symmetric and asymmetric reflection geometries were performed. Fig. 6 summarizes the results of the CoPt film grown at 730 K. Fig. 6a, b shows $\theta/2\theta$ scans around the 111 and 222 reflections of CoPt, which are close to the substrate peaks. Only the 222 reflection can be separated from the 0012 substrate peak by a two-Gaussian fit. The position of the 222 CoPt peak leads to a spacing of the 222 planes equal to 1.088 Å, which is between the values of the $L1_0$-type ordered (1.087 Å) and fcc disordered (1.090 Å) bulk phase. It full width at half maximum leads to a normal coherence length equal to 6.5 nm which is close to the average height measured by STM (Fig. 5d). Fig. 6c–f shows the $\theta-\alpha/2\theta$ scans around the 112 and 113 reflections and their corresponding rocking curves: α represents the angle between the 111 and 112 (or 113) reflections. However, a separation of the 113 reflection from the 311 and 131 reflections is not possible due to the existence of the three variants independently of the twinning effect. In order to calculate the chemical order parameter, the integrated intensities around the 113 fundamental reflections are divided by 3. Note, that this assumes the same formation probability and the same degree of long-range order for the three variants as the 112 and 113 reflections were not measured for the two other variants accessible by rotating the sample with respect to [1 1 1] axis. The integrated intensities are corrected for absorption and Lorentz factors taking into account the width of the rocking curves. The 113 and 112 intensities are proportional to the square of the structure factors equal to $F_{113} = 2(F_{Pt} + F_{Co})$ and $F_{112} = 2(F_{Pt} - F_{Co})\eta$. η is the chemical order parameter equal to 1 for a completely ordered alloy and $F_{Pt}(F_{Co})$ are the form factors of Pt(Co) species. For CoPt grown at 730 K, the ratio between the 113

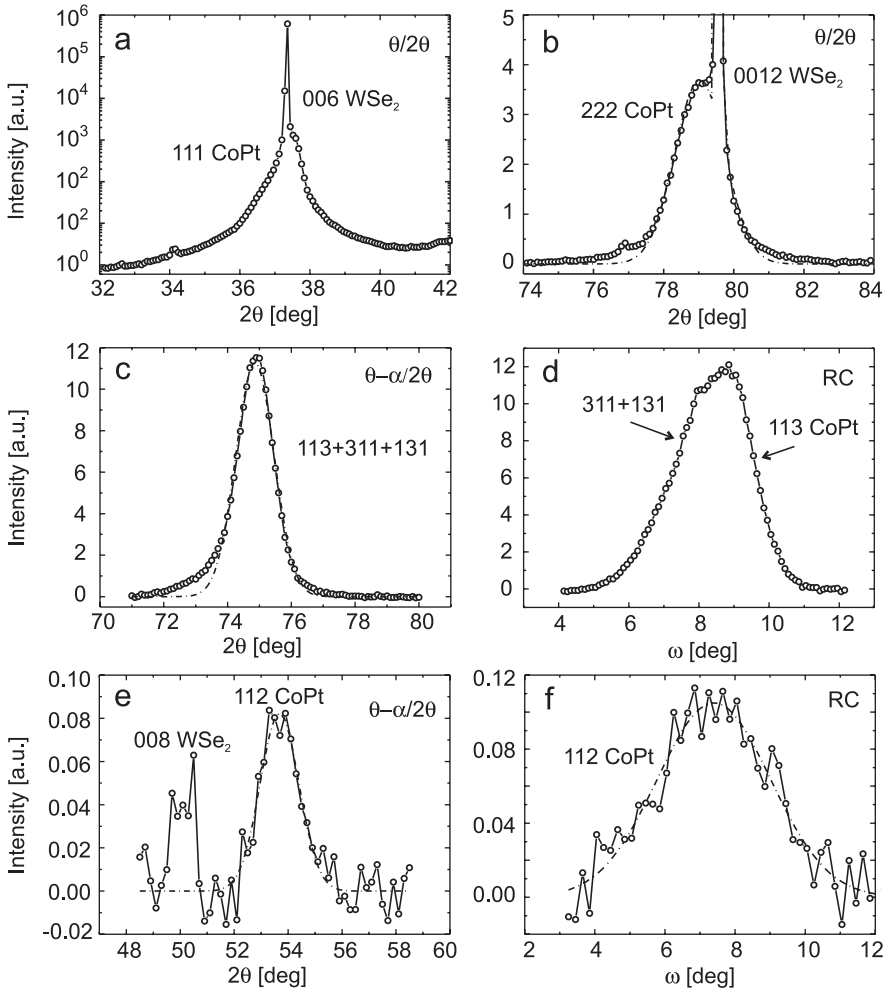

Fig. 6. XRD measurements in symmetric and asymmetric reflection geometries carried out on CoPt(1 1 1) film grown at 730 K. $\theta/2\theta$ scans around (a) 111 and (b) 222 reflections of CoPt(1 1 1). $\theta-\alpha/2\theta$ scans and corresponding rocking curves around 113 (c, d) and 112 (e, f) reflections of CoPt(1 1 1). α represents the angle between the [1 1 1] and [1 1 3] (or [1 1 2]) directions. Note that the three-index notation is used to identify reflections coming from the substrate and nanostructures.

and 112 intensities leads to a chemical order parameter of 0.35 ± 0.05, which is close to the value reported in Ref. [17].

The a and c lattice parameters of the tetragonal phase are deduced from the peak positions of the 222 and 112 reflections, since the 113 reflection while more intense is mixed with the 311 and 131 reflections. As expected for a low degree of ordering, a reduced tetragonality ratio is found ($a = 3.78$ Å and $c = 3.75$ Å) compared to that in the fully ordered phase ($a = 3.806$ Å and $c = 3.684$ Å).

For the film prepared at 570 K the same degree of the chemical ordering of 0.35 ± 0.05 was estimated. It is expected, that the segregation of Se at elevated temperatures during deposition of CoPt on WSe_2(0 0 0 1) and surface disorder effects associated with a large surface-to-volume ratio might limit the long-range order. The same effect was observed for the $CoPt_3$ alloy grown on WSe_2, where the maximum value for the ordering parameter was found to be ~0.65 at the wide temperature range of 470–870 K. For the CoPt film grown at 470 K, the width of the 222 reflection leads to a normal coherence length of about 4 nm consistent with the STM observations (Fig. 5d). Unfortunately, the average long-range chemical order parameter could not be determined for the sample, because the 112 reflection could not be detected by X-ray diffraction.

4. Magnetic properties

Magnetic properties of the CoPt deposits were investigated by SQUID magnetometry carried out at various temperatures. The effect of thermal activation and magnetic relaxation was studied by measuring zero-field and field cooling (ZFC/FC) curves. Note that a small in-plane field of 30 mT was used for this study. For the CoPt sample grown at room temperature, the magnetic behavior is consistent with the structural isotropy of the disordered fcc CoPt(1 1 1) structure. The hysteresis loops measured at 10 K show soft magnetic properties with small in-plane and out-of-plane coercivities of 20 and 60 mT, respectively (Fig. 7a, b). Due to the film morphology (see Fig. 5a), the grains are expected to be strongly exchange coupled leading to an enhanced thermal stability. This behavior is also indicated in the ZFC and FC curves (Fig. 8a), which

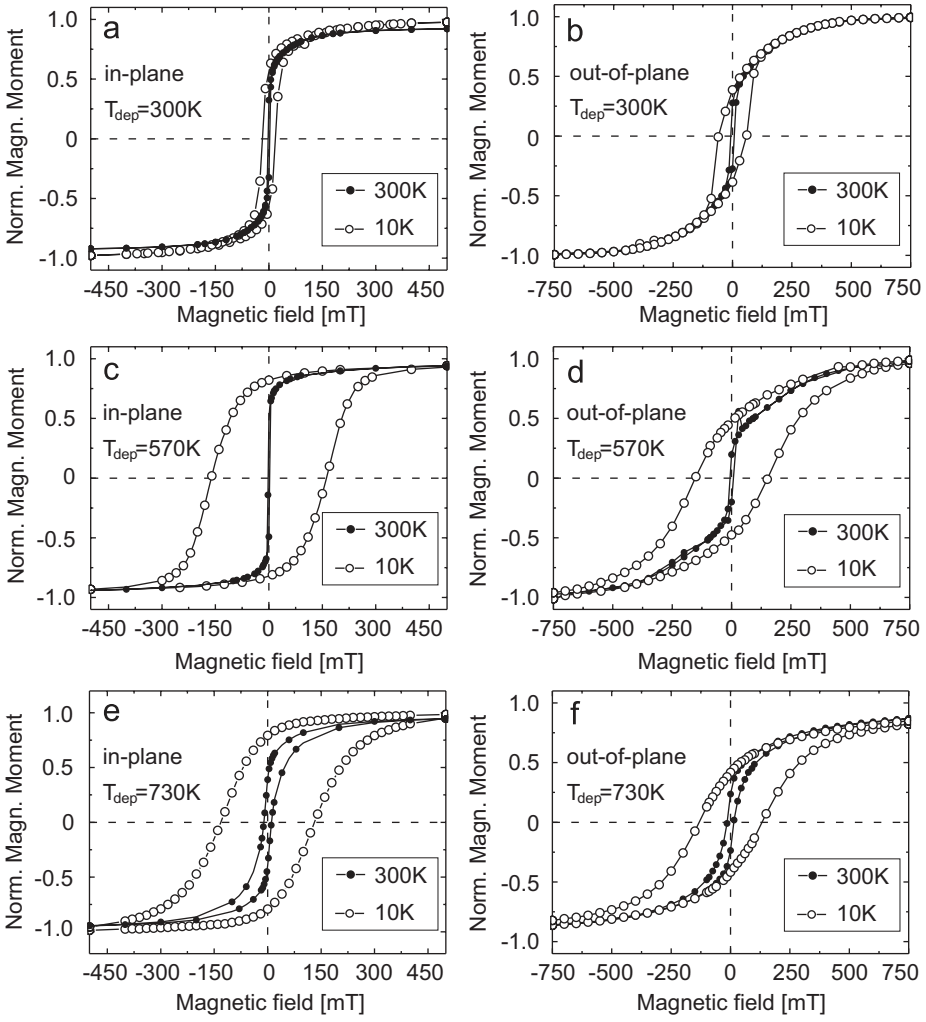

Fig. 7. SQUID hysteresis loops of 3-nm-thick CoPt(1 1 1) films grown on WSe_2(0 0 0 1) at (a, b) 300 K, (c, d) 570 K and (e, f) 730 K. Hysteresis loops were measured in the in-plane and out-of-plane geometry.

show no strong indication of a superparamagnetic state despite of the weak magnetic anisotropy and the small size of the individual grains.

In contrast, CoPt films grown at 570 K reveal a characteristic superparamagnetic transition at about 200 K with a broad transition (Fig. 8b) which is related to the rather large grain size distribution, variation in the degree of chemical order and thus magnetic anisotropy in the grains. It is expected that the grains are strongly magnetically exchange decoupled due to their morphology revealing more isolated grain structures. Hysteresis loops measured at 10 K (Fig. 7c, d) prove the presence of the partial chemical order in the CoPt grains which is associated with an enhancement of the in-plane and out-of-plane coercivity of up to 160 mT revealing an easy axis of magnetization in the film plane forced by the shape anisotropy.

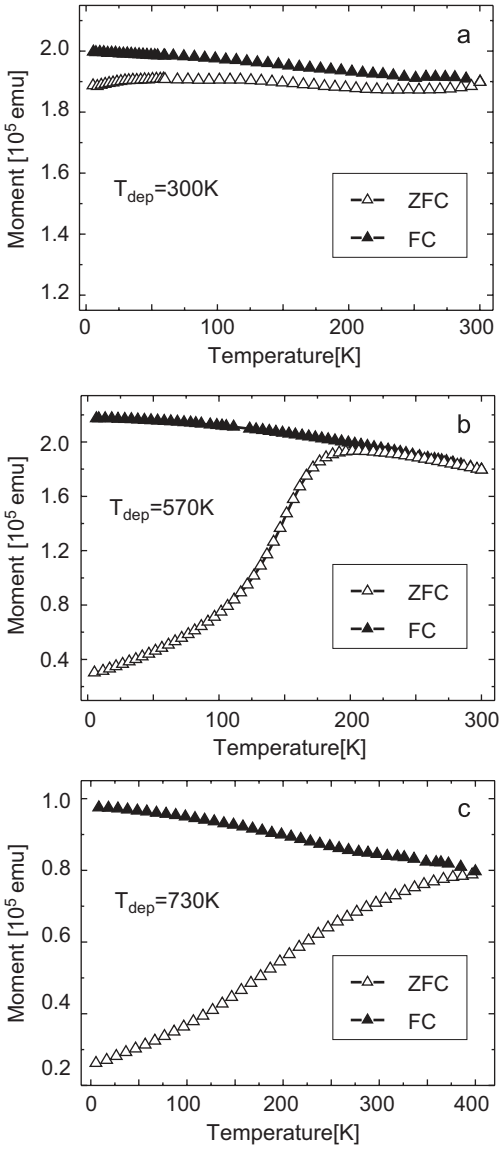

Fig. 8. ZFC/FC curves measured in the in-plane geometry at 30 mT for 3-nm-thick CoPt(1 1 1) films deposited at (a) 300 K, (b) 570 K, and (c) 730 K on WSe_2(0 0 0 1).

The SQUID data presented in Fig. 7e, f indicate that for the film prepared at 730 K the easy axis is still lying in the film plane at 10 K. However, the drastic change in shape and size of the grains will modify the shape anisotropy contribution in this case. Based on our X-ray measurements no increase of the chemical order was found by increasing the temperature from 570 to 730 K. Consequently, the uniaxial anisotropy along $\langle 0\,0\,1 \rangle$ has to be similar in both deposits. FC and ZFC curves indicate a superparamagnetic behavior with a broad distribution of blocking temperatures which is shifted to higher temperatures even above room temperature mainly due to the larger grain size.

5. Conclusion

Co-deposition of Co and Pt on WSe_2(0 0 0 1) leads to the formation of a single crystalline fcc CoPt alloy with (1 1 1) orientation even for the sample prepared at room temperature. Deposition at elevated temperatures induces $L1_0$ chemical order starting at 470 K accompanied with a pronounced increase in CoPt grain size and change in grain morphology. However, the increase in the deposition temperature to 730 K does not enhance the order parameter, which is about 0.35. It is expected, that the segregation of Se at elevated temperatures during deposition of CoPt on WSe_2(0 0 0 1) and surface disorder effects associated with a large surface-to-volume ratio might limit the long-range order. Similar effects have been reported for $CoPt_3$(1 1 1) [11], $CrPt_3$(1 1 1) [24], and FePt(1 1 1) [19] alloys grown on WSe_2(0 0 0 1). In contrast to $CoPt_3$ films grown on WSe_2(0 0 0 1) at room temperature, magnetic studies on CoPt do not reveal perpendicular magnetic anisotropy caused by the short-range chemical order. However, different magnetic behaviors are observed for CoPt films grown at various temperatures ranging from exchanged coupled continuous films when grown at room temperature to a superparamagnetic behavior at elevated deposition temperatures consistent with the related film morphology and the degree of chemical order.

Acknowledgments

The authors would like to thank A. Barth and I.L. Guhr (University of Konstanz) for assistance in SQUID measurements. Financial support was provided by the Deutsche Forschungsgemeinschaft through the SFB 513 and the Deutscher Akademischer Austauschdienst (Procope). Allocation of beamtime on the French CRG BM02 beamline at the ESRF is gratefully acknowledged.

References

[1] D. Weller, A. Moser, IEEE Trans. Magn. 35 (1999) 4423.
[2] K.R. Coffey, M.A. Parker, J.K. Howard, IEEE Trans. Magn. 31 (1995) 2737.

[3] Y.-N. Hsu, S. Jeong, D.E. Laughlin, D.N. Lambeth, J. Appl. Phys. 89 (2001) 7068.
[4] A.-C. Sun, P.C. Kuo, J.-H. Hsu, H.L. Huang, J.-M. Sun, J. Appl. Phys. 98 (2005) 076109.
[5] B.B. Maranville, F. Hellman, Appl. Phys. Lett. 81 (2002) 4011.
[6] V. Karanasos, I. Panagiotopoulos, D. Niarchos, H. Okumura, G.C. Hadjipanayis, Appl. Phys. Lett. 79 (2001) 1255.
[7] H. Zeng, M.L. Yan, N. Powers, D.J. Sellmyer, Appl. Phys. Lett. 80 (2002) 2350.
[8] T. Shima, T. Moriguchi, S. Mitani, K. Takanashi, Appl. Phys. Lett. 80 (2002) 288.
[9] H. Bernas, J.-Ph. Attane, K.-H. Heinig, D. Halley, D. Ravelosona, A. Marty, P. Auric, C. Chappert, Y. Samson, Phys. Rev. Lett. 91 (2003) 077203.
[10] M. Albrecht, A. Maier, F. Treubel, M. Maret, R. Poinsot, G. Schatz, Europhys. Lett. 56 (2001) 884.
[11] A. Maier, B. Riedlinger, F. Treubel, M. Maret, M. Albrecht, E. Beaurepaire, J.-M. Tonnerre, G. Schatz, J. Magn. Magn. Mater. 240 (2002) 377.
[12] P.W. Rooney, A.L. Shapiro, M.Q. Tran, F. Hellman, Phys. Rev. Lett. 75 (1995) 2843.
[13] M. Maret, M.C. Cadeville, R. Poinsot, A. Herr, E. Beaurepaire, C. Monier, J. Magn. Magn. Mater. 166 (1997) 45.
[14] M. Maret, unpublished results.
[15] R. Boom, F.R. de Boer, A.K. Niessen, A.R. Miedema, Physica B 115 (1983) 285;
A.K. Niessen, A.R. Miedema, F.T. de Boer, R. Boom, Physica B 151 (1988) 401.
[16] R.F.C. Farrow, D. Weller, R.F. Marks, M.F. Toney, S. Hom, G.R. Harp, A. Cebollada, Appl. Phys. Lett. 69 (1996) 1166.
[17] O. Ersen, V. Parasote, V. Pierron-Bohnes, M.C. Cadeville, C. Ulhaq-Bouillet, J. Appl. Phys. 93 (2003) 2987.
[18] D. Makarov, R. Pallesche, M. Maret, T.C. Ulbrich, G. Schatz, M. Albrecht, Surf. Sci. 601 (2007) 2032.
[19] M. Maret, B. Gilles, I. Guhr, B. Riedlinger, M. Albrecht, G. Schatz, E. Beaurepaire, Nanotechnology 15 (2004) 1590.
[20] R. Späh, U. Elrod, M. Lux-Steiner, E. Bucher, S. Wagner, Appl. Phys. Lett. 43 (1983) 79.
[21] S.H. El-Mahalawy, B.L. Evans, J. Appl. Cryst. 95 (1976) 403.
[22] T. Finteis, M. Hengsberger, Th. Straub, K. Fauth, R. Claessen, P. Auer, P. Steiner, S. Hüfner, P. Blaha, M. Vögt, M. Lux-Steiner, E. Bucher, Phys. Rev. B 55 (1997) 10400.
[23] CaRIne Crystallography Software 3.1.
[24] I.L. Guhr, B. Riedlinger, M. Maret, U. Mazur, F. Treubel, M. Albrecht, G. Schatz, J. Appl. Phys. 98 (2005) 063520.